JMEPEG (2011) 20:737–744
DOI: 10.1007/s11665-011-9910-7

1059-9495/$19.00

A Comparison of Different Nitinol Material Data Sources for Finite Element Analysis

Frank Nagl, Gerd Siekmeyer, Michael Quellmalz, and Andreas Schuessler

(Submitted June 25, 2010; in revised form January 7, 2011)

Nitinol (NiTi) is widely used for minimal invasive vascular implants due to its superelastic material behavior. Today computerized finite element analysis (FEA) modeling is a standard tool for the development of medical devices and an essential part of the product design and device approval process (X. Gong and A.R. Pelton, ABAQUS Analysis on Nitinol Medical Applications, *Proceedings of ABAQUS User's Conference*, New Port, Rhode Island, 2001, p 1; N. Rebelo and M. Perry, Finite Element Analysis for the Design of Nitinol Medical Devices, *Min. Invas. Ther. Allied Technol.*, 2000, 9(2), p 75). Quality of simulation depends on a multitude of parameters such as the mathematical material model and FE model generation (meshing). As such, a superior material data input is crucial in order to calculate the correct stress and strain conditions. In this study, we used different sources for material data input for our FE simulations. We compared simulated output versus the experimental results using a stent-like structure after various heat treatments. We used NiTi literature data, tensile data from raw as-supplied NiTi tubes as well as tensile and compression data from microtest samples which underwent stent-like processing for our FEA modeling. A FEA model of the diamond shape (DS) was constructed to quantify and visualize the force and motion response after applying different loading conditions similar to physiologic stress and strain. Force-deflection response of the virtual model was compared against the differently processed DS specimen. All results were put into a matrix in order to evaluate the quality of the different inputs for the FEA. The goal of this study was to demonstrate the importance of selecting and applying the correct material parameter inputs and to further show the importance of not just using given parameter, but also calibrating the values to get accurate results of FE simulations.

Keywords material selection, mechanical testing, nondestructive testing

1. Introduction

Shape memory alloy (SMA) is a common reference to metallic alloys capable of initial-form-recovering solid-solid phase transition as a result of applied external loads with thermomechanical nature (Ref 1, 2). This study examines the design variables associated with superelastic Nitinol (NiTi) for FEA modeling, and looks at design trade-offs within those variables. Through validated calibration and finite element analyses (FEA), this study shows the benefits that can be obtained by using optimized material data inputs.

In Fig. 1, the overall study design is outlined. During a first experimental investigation, we determined final material input parameters for FE simulations. Further calculations were conducted to verify the first FE simulation.

Microtensile test samples for uni-axial tensile testing have been laser cut from NiTi tubing. Two different heat treatments were applied on these specimen to demonstrate the difference in thermomechanical behavior of the NiTi material under load. Stress-strain curves were used to calibrate the FE material model parameter for a first diamond-shaped specimen design DS1. A uni-axial tensile and compression test of similar processed diamond-shaped specimen was used to compare and evaluate the accuracy of these simulations. Final material model input parameters were defined by only a small recalibration on the base of this direct comparison.

A second diamond-shaped specimen DS2 with modified tip design and two different applied heat-treatment processes was used to verify the final material input parameters of the first FE simulations.

2. Materials and Methods

The microtensile test samples and diamond-shaped specimen (Fig. 2) were cut from as-drawn NiTi tubing. Two different thermomechanical heat-treatment processes were applied at 475 and 505 °C (referred to lower and higher processing) to achieve a similar final Austenite finish (Af) temperature of 25 ± 3 °C. Specimen was later on grouped according to their heat-treatment process as a different heat-treatment process will change the mechanical material characteristics under load (Ref 3, 4).

This article is an invited paper selected from presentations at Shape Memory and Superelastic Technologies 2010, held May 16-20, 2010, in Pacific Grove, California, and has been expanded from the original presentation.

Frank Nagl, Gerd Siekmeyer, and **Michael Quellmalz**, Acandis GmbH & Co. KG, Theodor-Fahrner-Straße 6, 75177 Pforzheim, Germany; and **Andreas Schuessler**, ADMEDES Schuessler GmbH, Rastatter Str. 15, 75179 Pforzheim, Germany. Contact e-mail: fnagl@acandis.com.

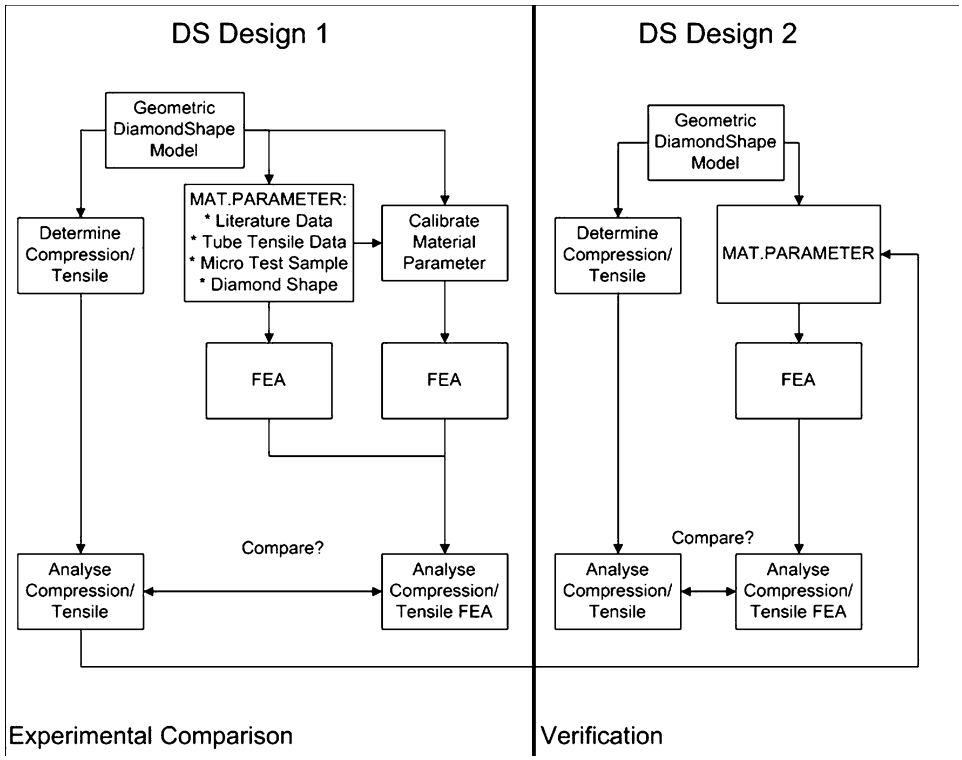

Fig. 1 Overall study design: 1. experimental comparison of different material input parameter sets (left). 2. Verification of results with a different specimen design (right). DS1: DiamondShape 1 and DS2: DaimondShape 2

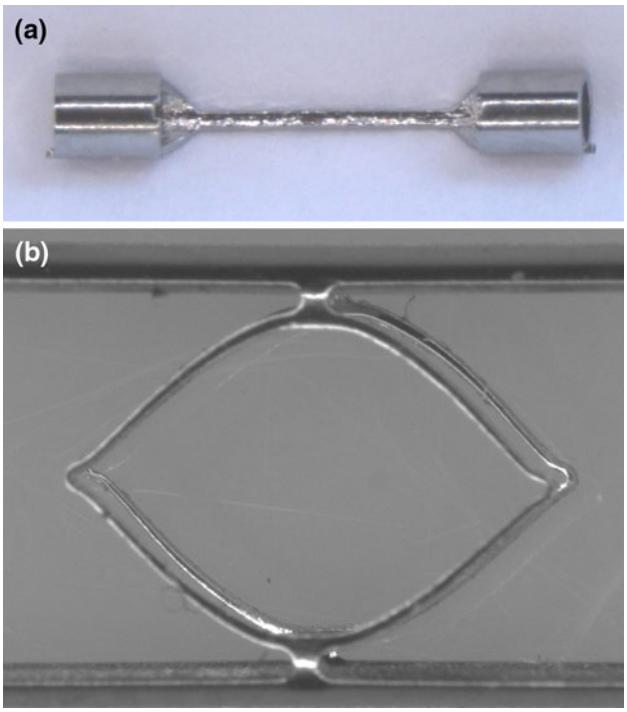

Fig. 2 Overview of tensile test specimen: (a) microtensile test sample and (b) diamond-shaped test specimen

3. Tensile Test Methods

Tensile testing of the microtensile test samples and diamond-shaped specimen were conducted on a Zwick Roell Z005 tensile tester according to ASTM F2516. A diamond-shaped specimen fixture for tensile testing is shown in Fig. 3 (side view). Specimen were elongated and compressed to ±1.5 mm.

4. Finite Element Analysis

Computerized FE simulations used the commercial FE solver ABAQUS version 6.9 (© Simulia 2009). In this software package a user material model (UMAT) for superelastic SMAs is included. The principle behavior of such materials is shown in Fig. 4.

FE models for the microtensile test sample and diamond-shaped specimen are based on the CAD drawings for manufacturing. All dimensions are measured by microscopy (Zeiss Discovery®). For the FE model, a mesh refinement of at least four elements across the strut width, four elements over the wall thickness and six elements for a 90° arc have been chosen. This refinement is supposed to deliver good solution accuracy in combination with short processing time for the calculation runs (Ref 6).

5. Material Parameter Calibration

The used method for the calibration is an iterative modification of the main parameters of the material model (Table 1) to simulate a certain loading condition. A tensile test with identical loading conditions is performed and the resulting stress-strain curve is compared to the FE calculated results. For further details of the material constitutive model refer to (Ref 5).

Fig. 3 Diamond-shaped specimen and tensile test setup

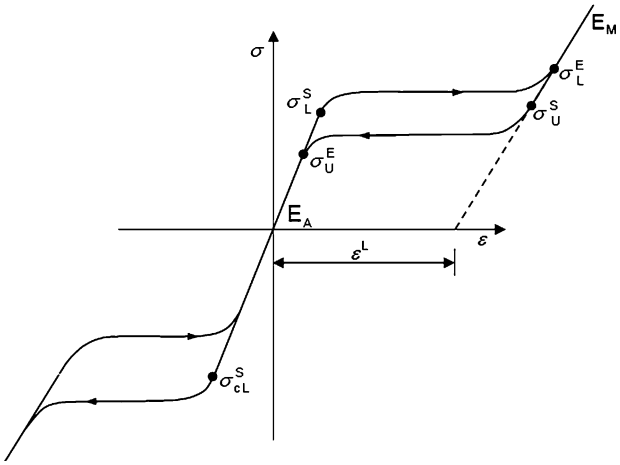

Fig. 4 Parameter for stress-strain behavior of the ABAQUS UMAT for superelastic shape memory alloys (Ref 5)

Table 1 List of parameter for the material calibration

EA	Austenite elasticity
EM	Martensite elasticity
ε_L	Transformation strain
σ_{LS}	Start of transition loading
σ_{LE}	End of transition loading
σ_{US}	Start of transition unloading
σ_{UE}	End of transition unloading

The iterative calibration process was considered complete at the moment that the FE calculated stress-strain curve matched closely the tensile stress-strain behavior of the specimen (Fig. 5).

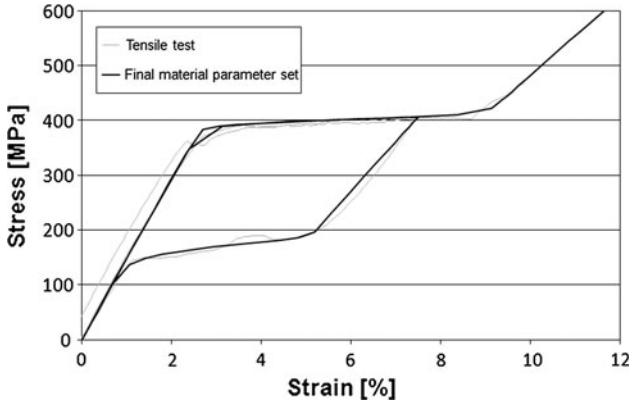

Fig. 5 Stress-strain plots of the final calibrated material parameter set; gray line: tensile test results micro test sample; black line: FE result with final calibrated material data

6. FE Simulation Data Sources and Models

For the first part of this study material input parameter sets have been determined from two different literature sources (Ref 7, 8) and from tensile testing of raw (as-drawn) NiTi tube material. Each material data source was calibrated to the behavior of the microtensile test samples.

The FE model (Fig. 6) was established based on the CAD drawings and dimensional measurements of the expanded diamond shape geometry (DS1).

The load during diamond shape testing was applied displacement controlled with the following loading profile:

1. Elongation +1.5 mm; 2. Compression −3 mm; 3. Elongation +1.5 mm.

Different FE-simulated deformation states of the DS1 FE model are shown in Fig. 7. The corresponding force-displacement plots are presented in Fig. 8.

To optimize the accuracy of the FE calculations the individual force-displacement behaviors of the FE simulations were compared to the mechanical tensile tests of the diamond-shaped specimen (DS1). A final calibration was applied to adjust the FE simulations of the heat-treated materials.

7. Results

Figure 9 compares the FE simulation results of the calibrated raw tube material with the tensile tests of lower- and higher-processed DS1 specimen.

A deviation in the resistance force of approximately 37% at a displacement of +1.5 mm can be seen for the comparison between raw tube material and higher-processed DS1. At the level of −1.5 mm displacement (compressive load) the maximum deviation is approx. 60%.

The deviation between lower-processed DS1 and raw tube material is quite low with approximately 7% during maximum compression, but much higher with approx. 22% under tensile loading.

All maximum deviations between the tensile tests and FE simulations of the DS1 specimen are presented in Table 2.

The results of the FE simulations of DS1 applying literature data input sets show a good conformity with the results of the tensile tests of higher-processed DS1 specimen.

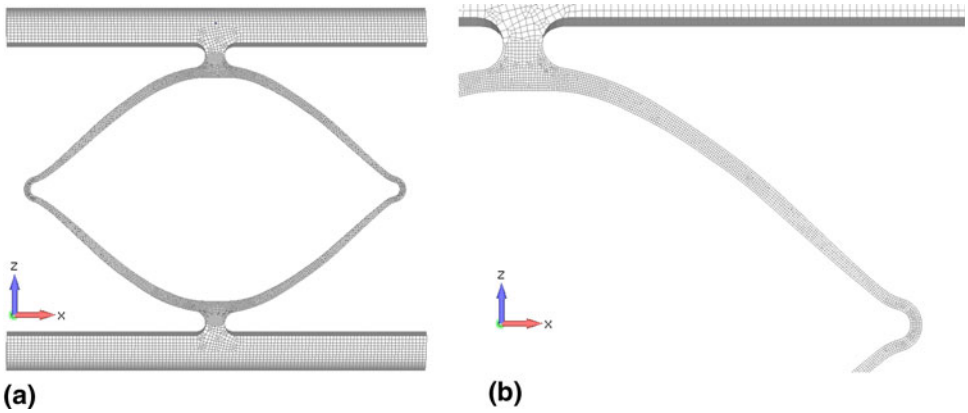

Fig. 6 FE model of the diamond-shaped specimen (DS1) based on CAD drawing and device measurement: (a) front view of the complete model; (b) detailed view of the model

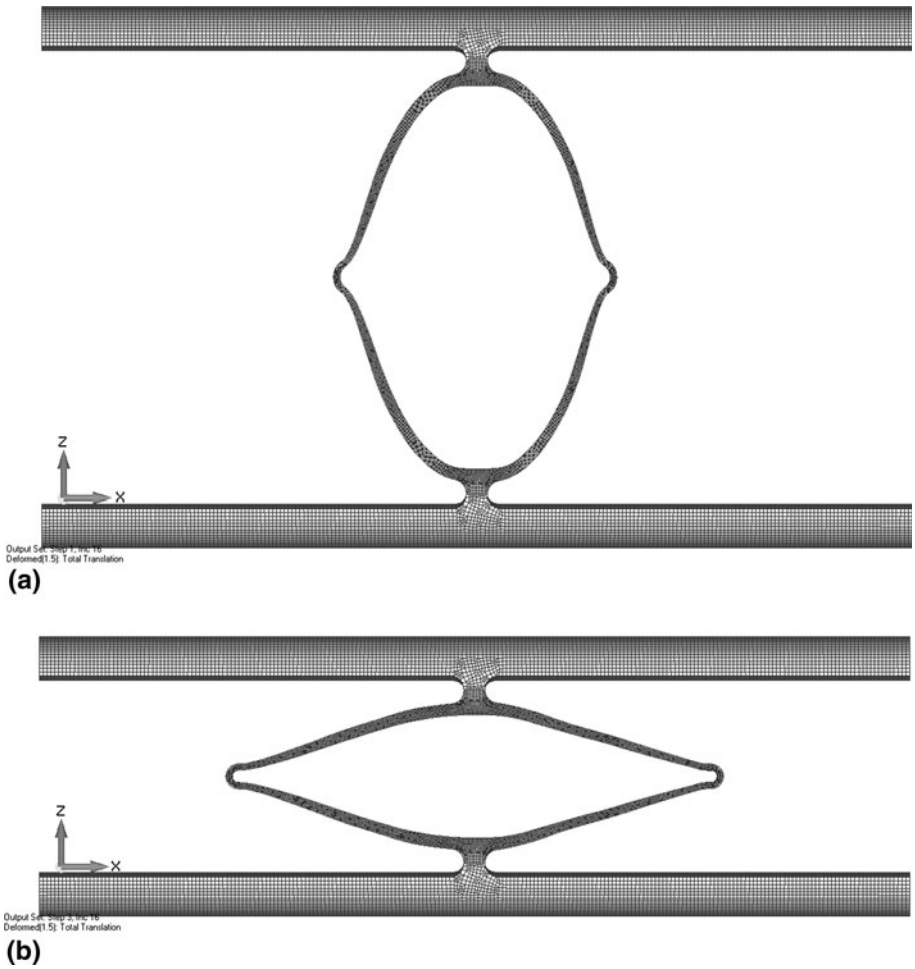

Fig. 7 FE-simulated deformations of the diamond-shaped specimen model (DS1): (a) maximum expanded state (+1.5 mm); (b) maximum compressed state (−1.5 mm)

The comparison to lower-processed DS1 specimen shows a constant but quite high deviation (about 22%). However, for compressive loading the FE simulation results for the literature and calibrated input sets demonstrate a very good accuracy with lower-processed DS1 specimen.

Figure 10 and 11 show results of the FE simulation of the DS2 model for verification after recalibrating the different material data inputs for higher- and lower-processed specimen.

In Table 3 the deviations of the simulated DS2 model behavior are compared to the tensile test data of the DS2

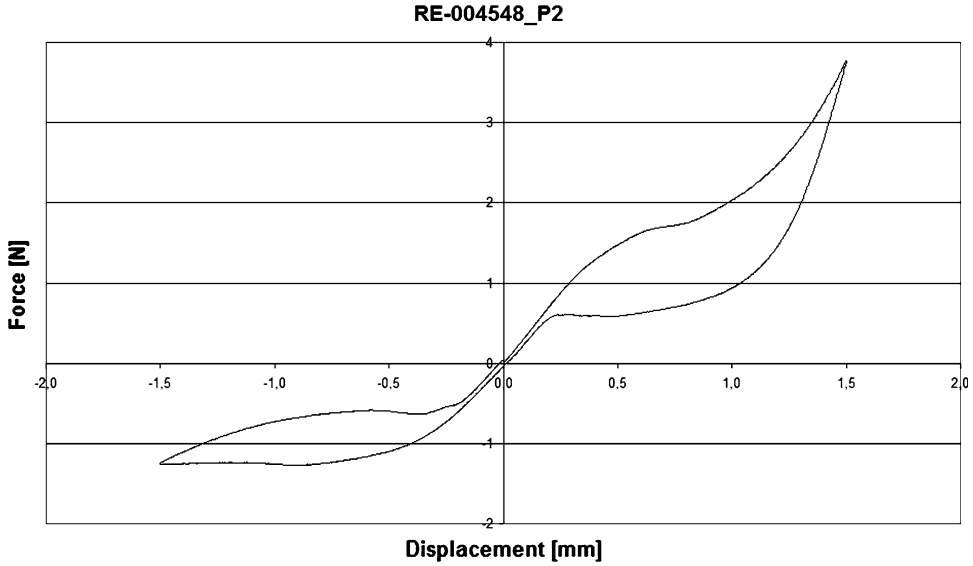

Fig. 8 Example of the resulting force displacement plot of a FE simulation with the described path controlled loading of the diamond shape specimen

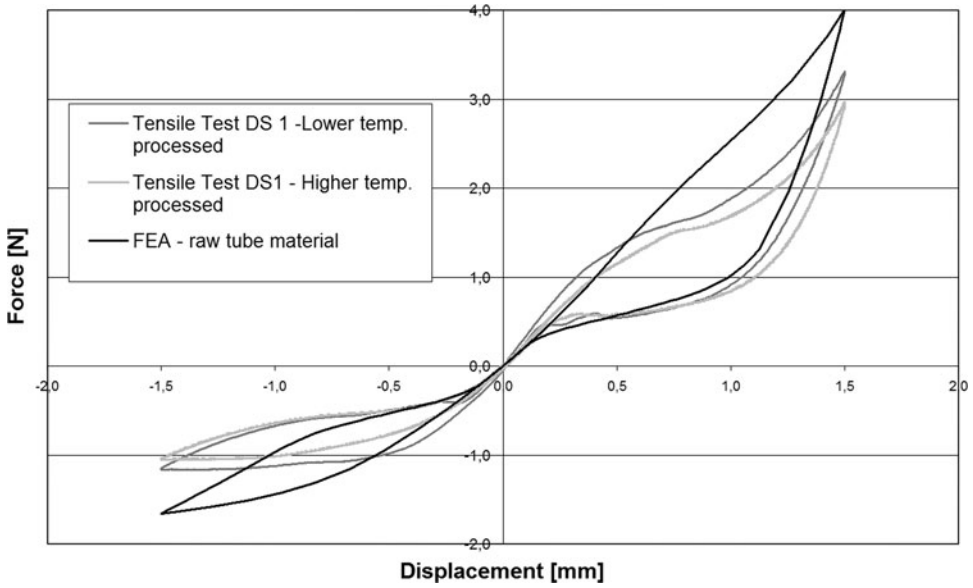

Fig. 9 Force-displacement plots of the FE simulated DS1 model from raw tube material vs. tensile test results of two differently heat-treated DS1 specimen; gray line: tensile test results of lower temperature processed (475 °C) specimen; gray dotted line: tensile test results of higher temperature processed (505 °C) specimen; black line: FE result with material data of raw tube material (no heat treatment)

Table 2 Comparison between the FE calculated and measured resistance force are summarized for the maximum compression and tensile loading condition with a displacement of ±1.5 mm of the DS1 specimen and FE model

	Max. deviation compared to tensile specimen			
	Tensile higher		Tensile lower	
	Displ. 1.5 mm	Displ. −1.5 mm	Displ. 1.5 mm	Displ. −1.5 mm
Lit. 1	9.3%	11.8%	22.4%	1.8%
Lit. 2	11.4%	13.7%	24.7%	3.6%
Raw tube	36.5%	60.8%	22.0%	46.4%
Calibrated higher	0.3%	26.5%		
Calibrated lower			22.4%	7.1%

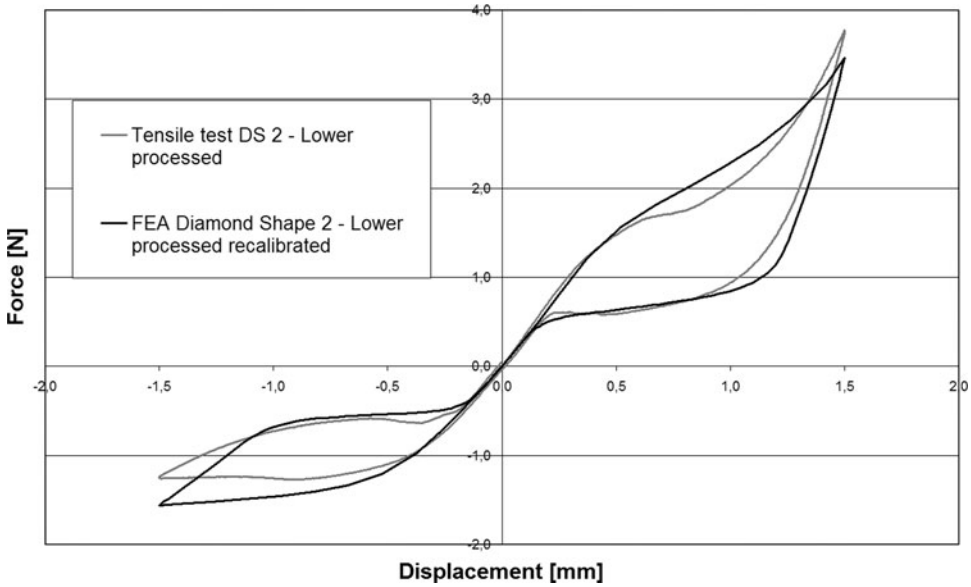

Fig. 10 Force-displacement plots of the FE simulated DS2 behavior with the lower-processed recalibrated material data set vs. the tensile test data of the lower-processed specimen; gray line: tensile test results of lower-processed specimen; black line: FE result with recalibrated lower material data set

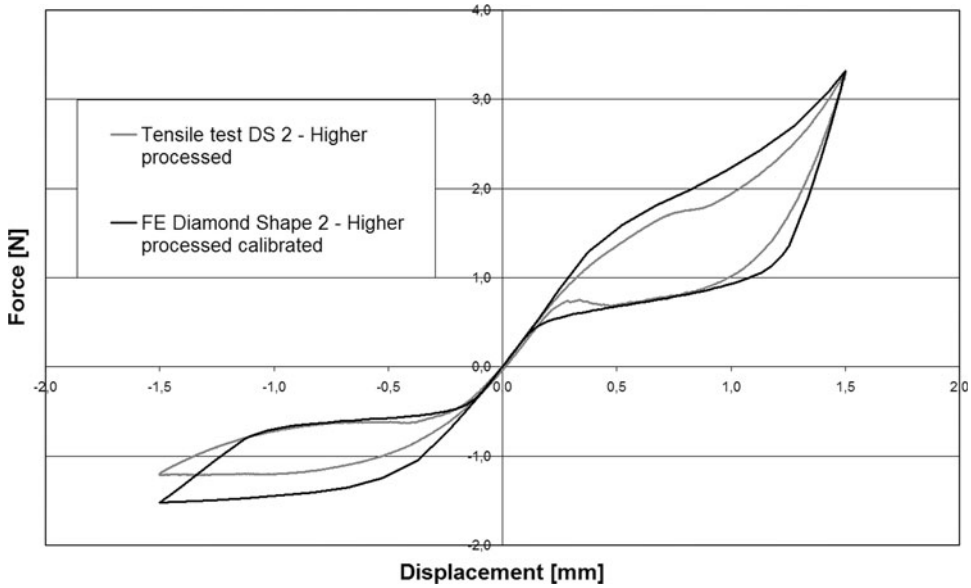

Fig. 11 Force-displacement plots of the FE simulated DS2 behavior with the higher-processed calibrated material data set vs. the tensile test data of the higher-processed specimen; gray line: tensile test results of higher-processed specimen; black line: FE result with calibrated higher-processed material data set

specimen. The deviation for the maximum tensile loading could be reduced to an average value of approximately 4.9% by this optimization process. The deviation of the resistance force under maximum compression loading is (with an average value of 0.32 N) approx. 26%.

In Fig. 12(a) and (b), the stress and strain distribution in the tip area of the DS1 with the calibrated higher-processed material parameter set and in Fig. 12(c) and (d) the stress and strain distributions of the DS1 specimen with the literature source two parameter input set are given.

The comparison of the stress and strain distributions shows that the level of maximum induced strain is approx. 0.59% lower for the higher-processed material parameter set compared to the literature source two-based parameter. In contrast, the maximum induced stress level is approx. 240 MPa higher using the calibrated higher-processed data compared to the literature source two input parameter set.

8. Discussion

In this study, the wide range of results from simulated mechanical behavior with various material data input sets for

Table 3 The deviations between the FE calculated and measured resistance force are summarized for the maximum compression and tensile loading condition with a displacement of ±1.5 mm of the DS2 specimen and FE model

	Max deviation calibrated higher temperature		Max deviation recalibrated lower temperature	
DS2	**Displ. 1.5 mm**	**Displ. −1.5 mm**	**Displ. 1.5 mm**	**Displ. −1.5 mm**
Calibrated higher temperature	2.5%	27.1%		
Recalibrated lower temperature			7.2%	25.4%

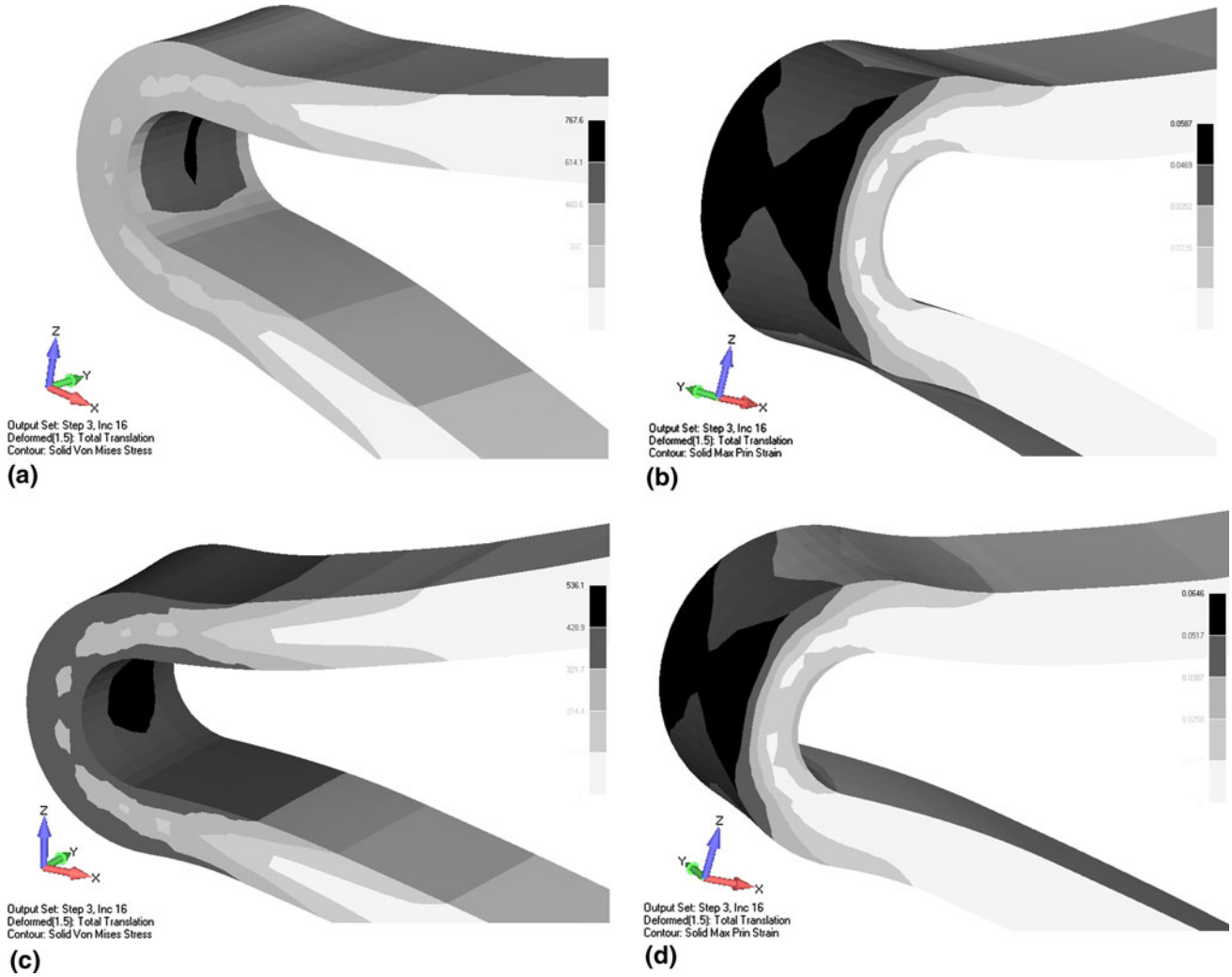

Fig. 12 (a) FE-calculated stress distribution of the DS1 specimen with the material input parameter set of the higher-processed material in the compressed state (−1.5 mm displacement) in MPa. (b) FE-calculated strain distribution of the DS1 specimen with the material input parameter set of the higher-processed material in the compressed state (−1.5 mm displacement). (c) FE-calculated stress distribution of the DS1 specimen with the material input parameter set of the material given in literature source two in the compressed state (−1.5 mm displacement) in MPa. (d) FE-calculated strain distribution of the DS1 specimen with the material input parameter set of the material given in literature source two in the compressed state (−1.5 mm displacement)

NiTi materials can be seen. It is therefore of utmost importance to carefully apply an optimization strategy for the material input data sets, if FEA is used for the simulation of radial forces and fatigue behavior. The comparison of the tensile test results with DS1 demonstrates that the use of more or less random material data can show a similar accuracy than parameter derived and calibrated on the basis of identical processed microtensile test material.

In contrast, if material input data sets are derived from raw tube material, the deviation is significantly different to the real behavior. In this case, a calibration process for the FE input parameters using processed specimen is highly recommended.

A further improvement of the FE results can be achieved, however, if an additional calibration procedure is conducted during the first verification step with the DS1 tensile test results. Unfortunately, this improvement is restricted only to the tensile

displacement range. There still remains a significant difference of maximum 27% between the force and displacement behavior of the DS2 specimen and the FE-derived results during compression.

The high deviation in compressed state should be reflected in another important parameter of the ABAQUS material UMAT model, which takes also the tensile and compression asymmetry of NiTi into account. The parameter σ_{cl}^{S} (start of transformation stress during loading in compression) allows a shift of the stress-strain behavior under compressive loading and not just a reflection (refer to Ref 5 for further details) if set not to zero.

In this study, the use of this parameter was not applied due to the fact that compression testing of uni-axial microtensile test samples or tube-shaped specimen with such small dimensions are not really practicable. This approach, however, would be possible, if the calibration is based on diamond-shaped specimen. These test samples will allow the measurement of tensile and compression force deflection response.

9. Conclusions

The quality of any FE simulation with NiTi materials can be significantly improved by applying a careful calibration process to identify the optimum material input data sets. It is possible to use simple uni-axial tensile tests for an accurate force-deflection simulation result; however, this will address mainly the quality for tensile loading conditions. Compressive loading conditions are rather inaccurate and can be calibrated only very limited from uni-axial tensile test data. This might result in high stress but low strain deviations like shown in Fig. 12(a)-(d) (for different processed materials).

Though it might be very dependent which kind of analysis is intended to be done. Force or stress-based simulations might need a more sophisticated calibration than just strain-based analysis of devices. Diamond shape testing as demonstrated in this study can be used for an optimum FEA simulation.

Acknowledgments

The authors would like to thank Frank Scherrible, Dr. Rainer Steegmüller, and Dr. Markus Wohlschlögel at Admedes Schuessler GmbH for laser cutting and providing technical feedback for this study.

References

1. X. Gong and A.R. Pelton, ABAQUS Analysis on Nitinol Medical Applications, *Proceedings of ABAQUS User's Conference*, New Port, Rhode Island, 2001, p 1
2. N. Rebelo and M. Perry, Finite Element Analysis for the Design of Nitinol Medical Devices, *Min. Invas. Ther. Allied Technol.*, 2000, **9**(2), p 75
3. K. Sadrnezhaad, F. Mashadi, and R. Sharghi, Heat Treatment of Ni-Ti Alloy for Improvement of Shape Memory Effect, *Mater. Manuf. Process.*, 1997, **12**, p 107–115
4. A. Bezrouk, J. Hanus, and J. Záhora, Temperature Characteristics of Nitinol Spiral Stents, *Scr. Med. (Brno)*, 2005, **78**(4), p 219–226
5. ABAQUS User Manual, ABAQUS Inc., 1080 Main Street, Pawtucket, Rhode Island 02860-4847
6. Best Practices for Stent Analysis (Support Answer 4516), Copyright Dassault Systèmes, www.3ds.com
7. D. Helm, "Formgedächtnislegierungen—Experimentelle Untersuchung, phänomenologische Modellierung und numerische Simulation der thermomechanischen Materialeigenschaften," Dissertation, Kassel, 2001
8. J.M. Mc Neanny et al., An Experimental Study of the Superelastic Effect in a Shape-Memory Nitinol Alloy Under Biaxial Loading, *Sci. Direct Mech. Mater.*, 2003, **35**, p 969–986